Correlated fluctuations of microparticles in viscoelastic solutions: Quantitative measurement of material properties by microrheology in the presence of optical traps

M. Atakhorrami,[1] J. I. Sulkowska,[1,*] K. M. Addas,[2,†] G. H. Koenderink,[1,‡] J. X. Tang,[2,§] A. J. Levine,[3,‖]
F. C. MacKintosh,[1] and C. F. Schmidt[1,¶]

[1]*Vrije Universiteit, Department of Physics and Astronomy and Laser Center, de Boelelaan 1081,
1081 HV Amsterdam, The Netherlands*
[2]*Department of Physics, Indiana University, 727 East Third Street, Bloomington, Indiana 47405, USA*
[3]*Department of Physics, University of Massachusetts, Amherst, Massachusetts 01003, USA*

The Brownian motions of microscopic particles in viscous or viscoelastic fluids can be used to measure rheological properties. This is the basis of recently developed one- and two-particle microrheology techniques. For increased temporal and spatial resolution, some microrheology techniques employ optical traps, which introduce additional forces on the particles. We have systematically studied the effect that confinement of particles by optical traps has on their auto- and cross-correlated fluctuations. We show that trapping causes anticorrelations in the motion of two particles at low frequencies. We demonstrate how these anticorrelations depend on trap strength and the shear modulus of viscoelastic media. We present a method to account for the effects of optical traps, which permits the quantitative measurement of viscoelastic properties in one- and two-particle microrheology over an extended frequency range in a variety of viscous and viscoelastic media.

PACS number(s): 83.50.−v, 83.60.Bc, 66.20.+d

I. INTRODUCTION

Complex fluids are commonly characterized by their viscoelastic properties. Considerable interest has in recent years also been devoted to biomaterials. These materials typically show a very complex time-dependent behavior related to their intrinsic length scales ranging from nm to μm. To probe this mechanical behavior over a wide frequency range, new rheological techniques are needed since most conventional rheometers are restricted to frequencies less than about 50 Hz due to the inertia of the macroscopic probes [1].

In part in an effort to increase the bandwidth (up to MHz), various active and passive (fluctuation based) microrheology (MR) techniques have been developed in recent years [2–11] that explore the viscoelastic properties of soft complex fluids by measuring the response of the medium to the motion of embedded micron-sized particles. In passive MR the samples are in thermal equilibrium and the probe particles execute Brownian motion. The complex response function of the particle is obtained via the fluctuation-dissipation theorem and a Kramers-Kronig integral, which relates the real and imagi-

nary parts of the response function. A generalized Stokes-Einstein (GSE) relation relates the complex shear modulus of the medium to the complex response function of the particle [2,4,5,12].

Microrheology in its simplest form can be done with a single probe particle (1PMR) where the rheological properties of the material are extracted from the displacement autocorrelation function of individual fluctuating particles. Such measurements probe the dynamics on length scales comparable to that of the particle. Two-particle microrheology (2PMR), on the other hand, uses the correlated fluctuations of two particles at a separation distance r, which can be much larger than the probe particle size and thus probe the mechanics of the medium on a length scale comparable to the interparticle separation [11,13–15].

Tracking of particles in transparent media can be done by video microscopy [16] which has the advantage of imaging $\sim$100 particles simultaneously and thereby rapidly obtaining good statistics. Standard video microscopy, however, is limited in frequency to 50/60 Hz with a spatial resolution of 10 to 50 nm. An alternative method giving higher spatial and temporal resolution is based on laser trapping of individual particles combined with interferometric displacement detection [4,5]. To apply this method to 2PMR, one uses a pair of focused laser beams to produce two optical traps in the sample holding a pair of (spherical) particles at a separation distance r [10,30,33,37]. Position fluctuations of each of the trapped particles are detected with quadrant photodiodes, with a bandwidth from $\sim$0.1 Hz to 100 kHz with a spatial resolution of better than 1 nm [17,5,18]. The detection range of the laser focus is on the order of only 1 μm. Therefore the particle has to be kept in focus if one wants to record motions over longer times. In a predominantly viscous solution the particle can be confined and moved about by the laser traps themselves. In a viscoelastic medium, such as a poly-

*Present address: Institute of Physics, Polish Academy of Sciences, Al. Lotnikow 32/46,02-668 Warszawa, Poland.

†Present address: The Rowland Institute at Harvard, 100 Edwin H. Land Blvd., Cambridge, Massachusetts 02142, USA.

‡Present address: Division of Engineering and Applied Sciences, Harvard University, 9 & 15 Oxford Street, Cambridge, Massachusetts 02138, USA.

§Present address: Physics Department, Brown University, 184 Hope Street, Providence, Rhode Island 02912, USA.

‖Present address: Department of Chemistry and Biochemistry, University of California, Los Angeles, California 90095, USA.

¶E-mail address: cfs@nat.vu.nl

mer solution or network, the probe particles are confined by the medium, and the laser has to be targeted on the particle. Even in that case, elevated laser power can be necessary to avoid shot noise when detecting particle motion at high frequencies.

Optical trapping introduces an additional force on the particles that is determined by the laser power rather than by the inherent mechanical properties of the medium. This will influence the thermal motions, so we must reexamine the relationship between the observed fluctuations of the particles and the rheological properties of the medium in which they are embedded. If not corrected for, the trapping potential introduces a systematic artifact in the magnitude of the storage modulus derived from the particle fluctuations, which can be dominant at low frequencies. In this paper we quantify both theoretically and experimentally the effects of the traps on the measured particle response functions in viscous and viscoelastic fluids using water and an aqueous solution of *fd* virus. We demonstrate that the response functions measured with 1PMR and 2PMR at low frequencies reflect a combination of the viscoelastic confinement by the medium and the trapping forces on the particles and we present a procedure to correct microrheology data for the trap effect.

II. MATERIALS

As an example of a purely viscous fluid we have used pure water. As an example of a viscoelastic medium we have used a 10 mg/ml solution of monodisperse filamentous virus particles, *fd* virus. The *fd* bacteriophages were prepared by a standard method [19], and details are described elsewhere [20]. The concentrated stock solution of virus rods was diluted to 10 mg/ml at pH 7 by adding a buffer solution with an ionic strength $I = 50$ mM (5 mM imidazole, 1 mM NaN_3, and 46.5 mM KCl).

As probe particles we used silica beads of radius $R = 0.58$ μm$\pm 5\%$ (Van 't Hoff Laboratory, Utrecht University, Utrecht, Netherlands), diluted to a final volume fraction of $\sim 10^{-5}$. After mixing the particles with the water or the virus solutions, we pipetted the solutions into sample chambers with $a \sim 20$ μl volume, made of a coverslip and microscope slide attached with two narrow strips of double-stick tape (inner height ~ 70 μm). After filling, the sample chambers were sealed at both ends with Apiezon H vacuum grease (M&I Materials LTD, Manchester, UK).

III. EXPERIMENTAL METHOD

Two independent polarized laser beams with wavelengths $\lambda = 1064$ nm (cw, Nd:YVO$_4$, Compass, Coherent) and $\lambda = 830$ nm (diode laser, cw, IQ1C140, Laser 2000) provided a pair of optical traps in a custom-built light microscope [14,21]. A schematic sketch of the experiment is shown in Fig. 1 where two particles, labeled 1 and 2, at a separation distance r are trapped in the two laser foci. To avoid surface effects, particles were trapped at a minimum distance of 20 μm away from all chamber surfaces. The laser intensity was varied for each wavelength individually using $\lambda/2$ plates and polarizers placed in the laser paths. The position fluctua-
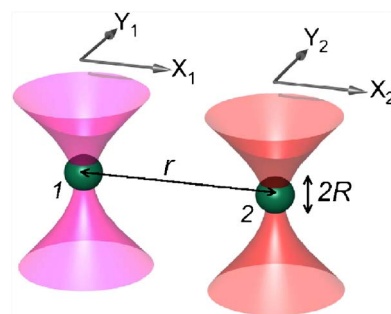

FIG. 1. (Color online) Schematic sketch of the two-particle microrheology experiment. A pair of silica particles (radius R) is trapped by a pair of laser traps at a separation distance r. The position fluctuations of each particle in the x and y directions are simultaneously detected with quadrant photodiodes. The cross-correlated position fluctuations are measured parallel and perpendicular to the line connecting the centers of the particles.

tions of each of the particles relative to the centers of the trap were detected in the x and y directions (normal to the optical axis) simultaneously using a back focal plane interferometric method with quadrant photodiode (QPD) detection [22]. The $\lambda = 1064$ nm laser was detected with a PIN photodiode operated with a reverse bias voltage of 100 V (10 mm diameter, YAG-444-4A, Perkin Elmer, Vaudreuil, Canada) [18], while the $\lambda = 830$ nm light was detected with a standard silicon-type PIN photodiode, operated with a reverse bias voltage of 15 V (10 mm diameter, Spot9-DMI, UDT, Hawthorne, CA). The particle position signals were digitized using an A/D board (195 kHz, ChicoPlus, Innovative Integration, Simi Valley, CA) at 195 kHz, antialias filtered at 100 kHz and recorded with a Labview program (National Instruments, Austin, TX, USA) for 80 sec per run. Data was averaged over 8 runs.

Position measurements were calibrated using the power spectrum method [23]. For *fd* solutions we used calibration data taken with beads from the same batch of particles, trapped in buffer. For water, we calibrated with the very same particles that were used for the measurements. The trap stiffness was obtained in water as a function of the laser power [23]. The laboratory temperature was stabilized to 21.4 ± 1 °C.

IV. DATA ANALYSIS METHOD

Thermal (Brownian) particle motions are exactly described by linear response theory [24]. We therefore relate the Fourier transform of the displacement $u_\alpha^{(j)}(\omega)$ of particle j (1 or 2) in direction α (x or y) to the Fourier transform of the applied force $F_\beta^{(k)}(\omega)$ applied to particle k in direction β via the response function $\chi_{\alpha\beta}^{(j,k)}(\omega)$ as: $u_\alpha^{(j)}(\omega) = \chi_{\alpha\beta}^{(j,k)}(\omega) F_\beta^{(k)}$. Here, $\omega = 2\pi f$ is the radial frequency and we have used the Einstein summation convention in which both coordinate directions (Greek indices) β and particle numbers (Latin indices) k are summed over. The single-particle response functions $\chi_{\alpha\beta}^{(1,1)}(\omega)$ and $\chi_{\alpha\beta}^{(2,2)}(\omega)$ refer to the displacement responses of particles 1 and 2 to forces applied to the same particle. The

$\chi_{\alpha\beta}^{(j,k)}(\omega)$ for $j \neq k$ refer to the inter-particle response functions, e.g., describing how particle 1 responds to forces on particle 2. Each of these, in general complex, response functions can be separated into real (in phase) and imaginary (out of phase) parts in the usual way: $\chi_{\alpha\beta}^{(j,k)}(\omega) = \chi_{\alpha\beta}'^{(j,k)}(\omega) + i\chi_{\alpha\beta}''^{(j,k)}(\omega)$.

In thermal equilibrium and in the absence of external forces the fluctuation-dissipation theorem [24] relates the imaginary part of the (single—or inter-particle) response functions to the equilibrium fluctuation spectrum of $u_\alpha^{(j)}(\omega)$

$$\chi_{\alpha\beta}''^{(j,k)}(\omega) = \frac{\omega}{2k_BT}S_{\alpha\beta}^{(j,k)}(\omega), \qquad (1)$$

where k_BT is the thermal energy and the $S_{\alpha\beta}^{(j,k)}(\omega)$ are given by

$$S_{\alpha\beta}^{(j,k)}(\omega) = \int \langle u_\alpha^{(j)}(t)u_\beta^{(k)}(0)\rangle e^{i\omega t}dt. \qquad (2)$$

In our experiments we chose a coordinate system with x and y spanning the plane perpendicular to the optical axis (laser propagation direction), and in which the x axis lies along the line connecting the centers of the two particles. In this coordinate system all $S_{\alpha\beta}^{(j,k)}$ are identically zero for $\alpha \neq \beta$ (here and throughout this paper we shall assume that the viscoelastic medium is homogeneous and isotropic in the absence of probe particles). For the remaining and only nonzero components of $S_{\alpha\beta}^{(j,k)}$ we introduce the shorthand notation: $S_\parallel \equiv S_{xx}^{(j,k)}$, $S_\perp^{(j,k)} \equiv S_{yy}^{(j,k)}$. We do not analyze particle fluctuations along the z axis, perpendicular to the focal plane. Such fluctuations would also be given by $S_\perp^{(j,k)}$ if neither the medium nor the laser trap breaks the axial rotational symmetry of the two-particle system. In practice, the laser trap does break this symmetry, as the effective trapping potential is broader along the optical axis than in the plane perpendicular to that axis. In the event that these $S_{zz}^{(j,k)}$ correlations were measured, the resulting data could be analyzed using a trivial extension of the theory presented in this work.

At the risk of only apparent ambiguity, we shall also use a shorthand notation for the single-particle correlation functions, in which $S_\parallel^{(j)} \equiv S_\parallel^{(j,j)}$ and $S_\perp^{(j)} \equiv S_\perp^{(j,j)}$. Furthermore, in a medium that respects time-reversal invariance (assumed hereafter), all correlation functions must be symmetric under time reversal so that $S_\parallel^{(1,2)}(\omega) = S_\parallel^{(2,1)}(\omega) \equiv S_\parallel(\omega)$ and correspondingly for $S_\perp$. Thus, there are six nonzero correlation functions $S_{\parallel,\perp}^{(j)}$ and $S_{\parallel,\perp}$ which can be used to directly determine the imaginary parts of the six corresponding response functions $\chi_{\parallel,\perp}^{(j)}$ and $\chi_{\parallel,\perp}$ for $j = 1, 2$ using the fluctuation-dissipation theorem. Finally, for isolated particles (i.e., in the absence of another particle trapped close by) in isotropic and homogeneous media, or for large separations between particles, the isotropy of the system requires that $S_\parallel^{(j)} = S_\perp^{(j)}$. In this case, the four $S_{\parallel,\perp}^{(j)}$ (or $\chi_{\parallel,\perp}^{(j)}$) reduce to just two correlation (response) functions $S^{(j)}$ (or $\chi^{(j)}$).

From the various imaginary parts of the response functions $\chi_{\alpha\beta}^{(j,k)}(\omega)$, we obtain the real parts (and hence, the full complex quantities) via a Kramers-Kronig integral [24,5]

$$\chi_{\alpha\beta}'^{(j,k)}(\omega) = \frac{2}{\pi}P\int_0^\infty \frac{\zeta}{\zeta^2 - \omega^2}\chi_{\alpha\beta}''^{(j,k)}(\zeta)d\zeta$$

$$= \frac{2}{\pi}\int_0^\infty \cos(t\omega)dt\int_0^\infty d\zeta\chi_{\alpha\beta}''^{(j,k)}(\zeta)\sin(t\zeta), \quad (3)$$

where P denotes a principal value integral. For isolated particles in the absence of optical traps, the complex response functions $\chi^{(j)}$ are related to the complex shear modulus G of inhomogeneous, isotropic and incompressible medium by a generalized Stokes-Einstein relation [25,4–6]

$$\chi^{(j)}(\omega) \to \alpha^{(j)}(\omega) = \frac{1}{6\pi RG(\omega)}, \qquad (4a)$$

where we have assumed the same particle radius R for both particles $j = 1, 2$, which is the case for our experiments. Here, we have introduced a new symbol α for the response functions, since it will be important to distinguish the *measured* response functions in the presence of traps (for which we shall consistently use χ), from those response functions that would be observed in the absence of traps (α). The latter characterize the part of the response due entirely to the medium, and they are thus the quantities of interest for rheology. Thus, we shall refer to these α as either *corrected* or *medium* response functions. The arrow in the above equation signifies that the measured response function χ directly reflects the *actual* rheology of the medium only in the absence of the trapping potentials.

Likewise, in the absence of traps, the inter-particle response functions $\chi_{\parallel,\perp}$ are given by generalizations of the Oseen tensor [6,12]

$$\chi_\parallel(\omega) \to \alpha_\parallel(\omega) = \frac{1}{4\pi rG(\omega)}$$

and

$$\chi_\perp(\omega) \to \alpha_\perp(\omega) = \frac{1}{8\pi rG(\omega)}, \qquad (4b)$$

where r is the separation between the particles. These expressions neglect inertia [29,33,34], which is a good approximation in the low frequency range studied here. While both of these expressions can be used to determine the modulus G, we find experimentally that the perpendicular channel is noisier than the parallel one.

In the presence of optical traps, additional forces are applied to the particles from the laser potentials. Thus, the displacements of each of the particle $u_\alpha^{(j)}(\omega)$ are modified by both trap potentials on the pair of particles. We model an optical trap as a Hookean spring characterized by a single isotropic trap stiffness or spring constant. In frequency representation, the additional trapping force in the αth direction on particle j is $-k^{(j)}u_\alpha^{(j)}(\omega)$, where $k^{(j)}$ is the trap stiffness holding particle j in the laser focus (here, no summation on j is implied). Thus, given an external force applied to that particle, $F_\alpha^{(j)}(\omega)$, the total force acting on it is $F_\alpha^{(j)}(\omega) - k^{(j)}u_\alpha^{(j)}(\omega)$. In terms of the (medium) response functions α, we can now write the displacements

$$u_x^{(1)}(\omega) = \alpha^{(1)}(\omega) \times [F_x^{(1)}(\omega) - k^{(1)} u_x^{(1)}(\omega)] + \alpha_\parallel(\omega)$$
$$\times [F_x^{(2)}(\omega) - k^{(2)} u_x^{(2)}(\omega)], \tag{5a}$$

and

$$u_x^{(2)}(\omega) = \alpha_\parallel(\omega) \times [F_x^{(1)}(\omega) - k^{(1)} u_x^{(1)}(\omega)] + \alpha^{(2)}(\omega)$$
$$\times [F_x^{(2)}(\omega) - k^{(2)} u_x^{(2)}(\omega)]. \tag{5b}$$

There is a similar pair of equations with x replaced by y and parallel by perpendicular.

Of course, the measured response functions χ are those that relate the $u_\alpha^{(j)}$ to $F_\alpha^{(j)}$ alone. These can be found by solving the above equations for $u_\alpha^{(j)}$. This results in expressions for the χ that are nonlinear in the α. For example, the linear response coefficient relating $u_x^{(1)}$ to $F_x^{(1)}$ is

$$\chi_{xx}^{(1,1)} = \chi_\parallel^{(1)}$$
$$= \frac{\alpha^{(1)} + k^{(2)} \alpha^{(1)} \alpha^{(2)} - k^{(2)} (\alpha_\parallel)^2}{1 + k^{(1)} \alpha^{(1)} + k^{(2)} \alpha^{(2)} + k^{(1)} k^{(2)} \alpha^{(1)} \alpha^{(2)} - k^{(1)} k^{(2)} (\alpha_\parallel)^2}. \tag{6a}$$

This nonlinear relationship should be distinguished from the fundamental *linear response* assumption that we make. Although the relationships among the various χ and α are nonlinear, we are still describing the linear response of the medium. Thus, for instance, we assume that forces and corresponding displacements are sufficiently small for the *linear* relationships in Eqs. (5a) and (5b) to be valid. In contrast, the higher-order terms beyond the leading term $\alpha^{(1)}$ do not depend on the amplitude of the displacement or force. These higher-order terms give relative contributions of order k/GR, kR/Gr^2, $k^2/(Gr)^2$, and $k^2/(GR)^2$, which depend on the trapping potentials k and the geometry of our experiments. Since these corrections do not depend on the amplitude of motion, they cannot be assumed to be small. Note also that the presence of the pair of traps breaks the rotational symmetry of the single-particle response, since

$$\chi_{yy}^{(1,1)} = \chi_\perp^{(1)}$$
$$= \frac{\alpha^{(1)} + k^{(2)} \alpha^{(1)} \alpha^{(2)} - k^{(2)} (\alpha_\perp)^2}{1 + k^{(1)} \alpha^{(1)} + k^{(2)} \alpha^{(2)} + k^{(1)} k^{(2)} \alpha^{(1)} \alpha^{(2)} - k^{(1)} k^{(2)} (\alpha_\perp)^2} \tag{6b}$$

differs from the expression in Eq. (6a) by terms second order in both trap stiffness and interparticle response. For the other particle, the corresponding expressions can be obtained by interchanging indices 1 and 2. The inter-particle response functions are given by

$$\chi_{xx}^{(1,2)} = \chi_\parallel$$
$$= \frac{\alpha_\parallel}{1 + k^{(1)} \alpha^{(1)} + k^{(2)} \alpha^{(2)} + k^{(1)} k^{(2)} \alpha^{(1)} \alpha^{(2)} - k^{(1)} k^{(2)} (\alpha_\parallel)^2}, \tag{6c}$$

and

$$\chi_{yy}^{(1,2)} = \chi_\perp$$
$$= \frac{\alpha_\perp}{1 + k^{(1)} \alpha^{(1)} + k^{(2)} \alpha^{(2)} + k^{(1)} k^{(2)} \alpha^{(1)} \alpha^{(2)} - k^{(1)} k^{(2)} (\alpha_\perp)^2}. \tag{6d}$$

From an examination of the above equations, it is clear that in the limit of vanishing trapping potentials, the experimentally measured response functions χ reduce to the appropriate medium response functions α. These latter response functions, which are thus (in the presence of optical traps) not directly accessible via experiment, need to be known in order to determine the rheological properties of the medium. The experimentally accessible (measured) response functions χ, however, can be used to calculate the rheologically useful response functions α by inversion of the above equations. This inversion is facilitated by the observation that, within linear response, the parallel and perpendicular motions and/or response functions completely decouple. This, together with the symmetry properties mentioned above, leads to two separate sets, each of three nonlinear equations, that must be inverted. The resulting expressions for the parallel case are

$$\alpha^{(1)} = \frac{\chi_\parallel^{(1)} + k^{(2)} (\chi_\parallel)^2 - k^{(2)} \chi_\parallel^{(1)} \chi_\parallel^{(2)}}{1 - k^{(1)} \chi_\parallel^{(1)} - k^{(2)} \chi_\parallel^{(2)} - k^{(1)} k^{(2)} (\chi_\parallel)^2 + k^{(1)} k^{(2)} \chi_\parallel^{(1)} \chi_\parallel^{(2)}}, \tag{7a}$$

$$\alpha^{(2)} = \frac{\chi_\parallel^{(2)} + k^{(1)} (\chi_\parallel)^2 - k^{(1)} \chi_\parallel^{(1)} \chi_\parallel^{(2)}}{1 - k^{(1)} \chi_\parallel^{(1)} - k^{(2)} \chi_\parallel^{(2)} - k^{(1)} k^{(2)} (\chi_\parallel)^2 + k^{(1)} k^{(2)} \chi_\parallel^{(1)} \chi_\parallel^{(2)}}, \tag{7b}$$

$$\alpha_\parallel = \frac{\chi_\parallel}{1 - k^{(1)} \chi_\parallel^{(1)} - k^{(2)} \chi_\parallel^{(2)} - k^{(1)} k^{(2)} (\chi_\parallel)^2 + k^{(1)} k^{(2)} \chi_\parallel^{(1)} \chi_\parallel^{(2)}}. \tag{7c}$$

Similarly, for the perpendicular motion

$$\alpha_\perp = \frac{\chi_\perp}{1 - k^{(1)} \chi_\perp^{(1)} - k^{(2)} \chi_\perp^{(2)} - k^{(1)} k^{(2)} (\chi_\perp)^2 + k^{(1)} k^{(2)} \chi_\perp^{(1)} \chi_\perp^{(2)}}. \tag{7d}$$

Here, the additional pair of equations obtained for perpendicular motion can be obtained from Eqs. (7a) and (7b) by replacement of parallel with perpendicular throughout, which must give the same values for $\alpha^{(1)}$ and $\alpha^{(2)}$ in isotropic and homogenous media. We also note that among the various second-order correction terms, the ones involving the interparticle response are smaller than those involving the single-particle response by a factor of order $(R/r)^2$. Thus, for instance, the broken rotational symmetry of the single-particle response functions is expected to be small, even if second-order corrections due to the traps are otherwise relevant.

Here $k^{(1)}$ and $k^{(2)}$ are linearly dependent on the laser power and are known for each experiment. Specifically in our experiments $k^{(1)}$ is the trap stiffness of laser focus with $\lambda = 1064$ nm and $k^{(2)}$ is the trap stiffness of laser focus with $\lambda = 830$ nm.

Using Eqs. (4a) and (4b) we can extract the rheological properties of the medium as measured with one- and two-particle microrheology from the response functions α after correcting the measured response functions χ using Eqs. (7a)–(7d). Through this manipulation of the raw data we can thus prevent systematic errors that would otherwise be introduced by the trapping potentials.

V. RESULTS AND DISCUSSION

In this section we verify experimentally how the optical trapping potential modifies the complex particle response functions. We demonstrate how this effect can be corrected to for measure shear moduli of viscous and viscoelastic fluids with 1PMR and 2PMR. We first present results for 1PMR, then for 2PMR, in both cases for water and fd solutions. The *measured* response functions χ are compared with the predictions of Eqs. (6a)–(6d). Then, we obtain the corrected (medium) response functions α from the *measured* response functions using Eqs. (7a)–(7d). The shear moduli of the medium were calculated from the complex response functions after the correction for the traps. In order to demonstrate the necessity of correcting for trapping effects, we also calculated the (apparent) complex shear moduli without correcting for the trapping potential, i.e., directly from the correlation data using Eqs. (4a) and (4b).

We measured the auto- and cross-correlated displacement fluctuations of the two particles simultaneously in each sample and for every power setting, so that the trap stiffness of each individual optical trap was the same for the measured single- and inter-particles response functions. The silica particle pairs (radius $R=0.58$ μm) were trapped at a separation distance of $r=2.9$ μm. The strength of the laser traps was varied by changing the laser intensity from 3 to 200 mW (measured with a power meter before the incident beam entered the microscope path). Here we present the single-particle response functions measured with the laser trap of wavelength $\lambda=1064$ nm. Results for the second trap with $\lambda=830$ nm (not shown) were equivalent. The inter-particle response functions are similar in the parallel and perpendicular direction with respect to the line connecting the centers of the particles. We thus present just the results for parallel channel. Data are presented as a function of frequency $f=\omega/2\pi$.

A. One-particle microrheology (1PMR)

In 1PMR we measure the displacement autocorrelations of a single particle in a laser trap. The Fourier transform of this correlation function as defined in Eq. (1) for a thermally excited particle in a purely viscous fluid and laser trap takes the form of a Lorentzian [23,26]

$$S(2\pi f) = \frac{k_B T}{\gamma \pi^2 (f_c^2 + f^2)}, \qquad (8)$$

where f_c is the characteristic (corner) frequency which divides the curve $S(2\pi f)$ into two regimes. For frequencies $f < f_c$, the laser trap provides the dominant force on the particle and $S(2\pi f)$ is essentially constant, $S(2\pi f)$
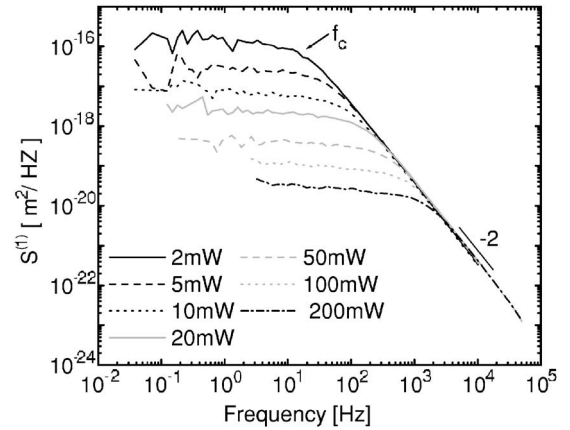

FIG. 2. Displacement autocorrelations of a particle trapped in water as a function of frequency $f=\omega/2\pi$. The laser intensity (wavelength $\lambda=1064$ nm) was varied between 3 and 150 mW. The corner frequency f_c changes with laser intensity; the high frequency power-law slope is -2. Laser noise (increasingly prominent for stronger confinement at higher powers) was cut off at the low-frequency end of the curves.

$\sim S_0(2\pi f)=4\gamma k_B T/k^2$. At higher frequencies $f\gg f_c$, hydrodynamic drag forces acting on the particle dominate the trapping forces and $S(f)$ decays as $1/f^2$, which is equivalent to free Brownian motion in a purely viscous solution. The trap stiffness can be calculated most conveniently from the corner frequency as $k=2\pi f_c\gamma$, where $\gamma=6\pi\eta R$ is the Stokes drag on a spherical particle with radius R.

Figure 2 shows a log-log plot of the position autocorrelation $S^{(1)}(2\pi f)$ of a silica particle ($R=0.58$ μm) trapped in water at different laser powers. The laser intensity was varied from 3 to 150 mW, corresponding to corner frequencies between 30 Hz and 1 kHz. As expected, the corner frequency shifts to higher frequencies as the trap stiffness increases. Also, the area under $S^{(1)}(2\pi f)$ decreases as the particle is more tightly trapped (larger k) indicating that the rms amplitude of the position fluctuations decreases in accordance with the equipartition theorem. At high frequencies, where the particle is freely diffusing, all the measurements for different laser powers fall onto one line with a power-law slope of -2. The sampling frequency for low laser powers of 3 and 7 mW was 20 kHz, while for higher laser intensities of 15, 25, 70, 150, and 200 mW a sampling rate of 100 kHz was used.

Figure 3 shows that the trap stiffness depends linearly on laser intensity. The quoted laser powers were measured before the laser beams entered the microscope objective and are about a factor of 2 higher than power in the sample, with the absorption of light being different for the two different wavelengths [27] and the power passed through the objective also dependent on how much of the laser beam overfills the objective back aperture. Due to slightly varying alignments, the quoted laser powers are only a rough indication of trapping strengths and for calculations of the trap effect on the complex response functions, we used the measured trap stiffnesses, obtained from the corner frequencies of the autocorrelation spectra measured for the same silica particles in water.

In viscoelastic solutions the autocorrelation spectra are not Lorentzian, and we cannot fit for a corner frequency to
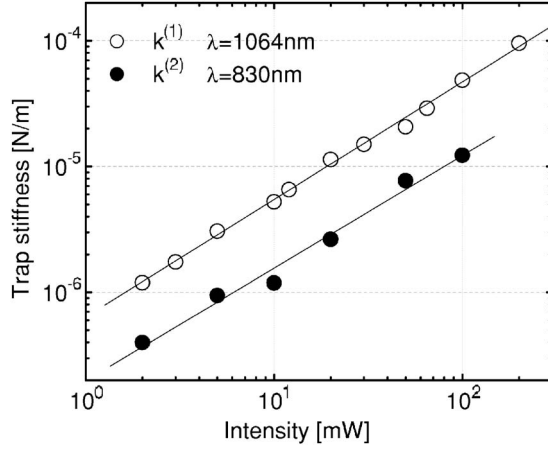
FIG. 3. Trap stiffnesses of two laser traps generated by independent lasers ($\lambda = 1064$ and 830 nm) measured from the fluctuations of two silica particles ($R = 0.58$ μm) in water. The trap stiffnesses increased linearly with the laser intensities (measured before the beams entered the objective) for both traps.

obtain the trap stiffness k for the same particle as used for the experiments. There are two alternative methods to find k, (i) one can trap a particle from the same batch at the same laser power in water, introducing an error due to particle polydispersity or (ii) one can use the low-frequency data points for $G'(\omega)$ to extract k provided that the low frequency apparent $G'(\omega)$ is dominated by the trap. The error of this method increases with the elastic modulus of the solution.

A prediction for the *measured* response function of one particle trapped in a laser focus in water can be calculated from Eqs. (6a) and (6b), using the known trap stiffness $k^{(1)}$ and $k^{(2)}$ in each measurement. From the stationary Stokes results [28], the response function of one particle in a simple viscous fluid of viscosity η and subject to no trapping potential is $\alpha^{(1)} = \alpha^{(2)} = 1/[6\pi R \eta(-i\omega)]$, while the inter-particle response function of two such particles along their centers is given by $\alpha_\parallel = 2\alpha_\perp = 1/[8\pi r \eta(-i\omega)]$ [29]. We insert these quantities in Eqs. (6a) and (6b) and obtain a theoretical prediction of the *measured* response function in water.

Figures 4(a) and 4(b) show log-log plots of the real and imaginary parts of the *measured* single-particle response function in water, compared to the predicted ones. The $\chi_\parallel'^{(1)}(2\pi f)$ and $\chi_\parallel''^{(1)}(2\pi f)$ are plotted for different laser intensities between 7 and 150 mW (same data as in Fig. 2). Figures 4(a) and 4(b), show very good agreement of the experimental data with the theoretical predictions with no adjustable parameters. In this calculation we used the trap stiffnesses $k^{(1)}$ and $k^{(2)}$ shown in Fig. 3. The filled symbols in Fig. 4(b) represent the imaginary part of the *medium* single-particle response function, $\alpha''^{(1)}(2\pi f)$, calculated from the *measured* one using Eq. (7a). The $\alpha''^{(1)}(2\pi f)$ thus obtained should be equal to the simple Stokes result for a viscous fluid of $1/[6\pi R \eta(-i2\pi f)]$ [grey line in Fig. 4(b)]. This is evidently the case at high frequencies for all the different laser powers, where all of the $\chi_\parallel''^{(1)} = \alpha''^{(1)}$ collapse onto the gray line. At lower frequencies, however, the $\chi_\parallel''$ diverge from the gray line in a power dependent way. The corrected response functions $\alpha''^{(1)}$ collapse onto the Stokes result except for
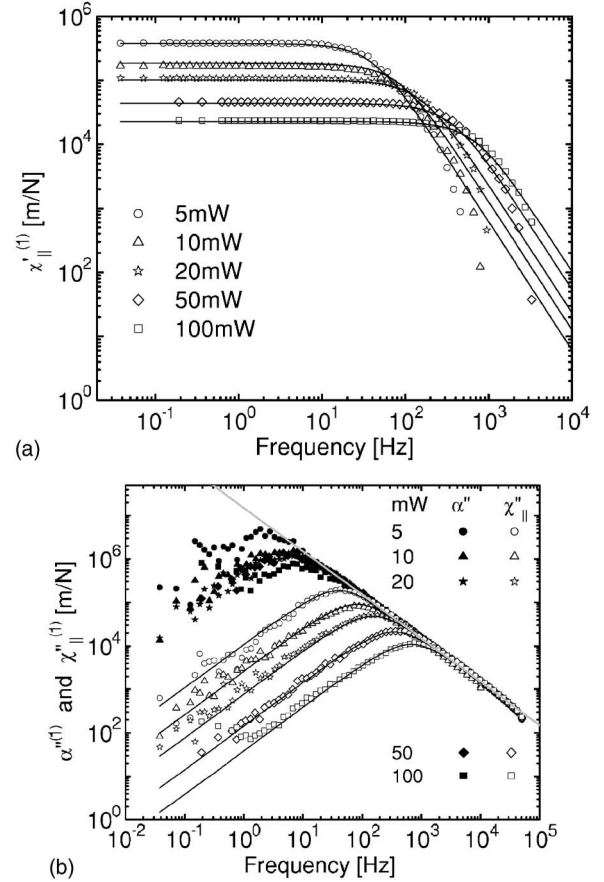

FIG. 4. Frequency dependence of (a) the real part $\chi_\parallel'^{(1)}$ and (b) the imaginary part $\chi_\parallel''^{(1)}$, of the *measured* single-particle response functions in water, for x displacements (empty symbols). The data agree well with theoretical prediction (solid dark lines) calculated from Eq. (6a) without any adjustable parameters. In (b) the solid symbols are *medium* response functions $\alpha''^{(1)}$, calculated from $\chi_\parallel'^{(1)}$ and $\chi_\parallel''^{(1)}$ by eliminating the trap effect according to Eq. (6a). The solid gray line is the expected Stokes result for a sphere in a viscous fluid.

some residual deviations for even lower frequencies. These are due to noise created by laser beam pointing fluctuations.

If one calculates an (apparent) shear modulus from the uncorrected response function $\chi_\parallel''$, one finds a nonzero storage modulus in the purely viscous medium, which is due to the laser traps. Figure 5 shows this apparent storage modulus as a function of frequency for different laser powers from 3 to 150 mW. Since water by itself does not have a storage modulus, the measured (frequency independent) values of 0.07 to 6.2 Pa are completely due to the laser trap and are therefore proportional to the laser intensity. The solid lines are calculated from the independently measured trap stiffnesses $k^{(1)}/(6\pi R)$.

Unlike water, solutions of semiflexible *fd* particles have a storage (*real*) component to the shear modulus. Thus the response functions measured with 1PMR contain a contribution of the *actual* elasticity of the medium as well as of the laser trap.

The autocorrelation function $S^{(1)}$ of one particle in an *fd* solution is plotted in Fig. 6 as a function of frequency
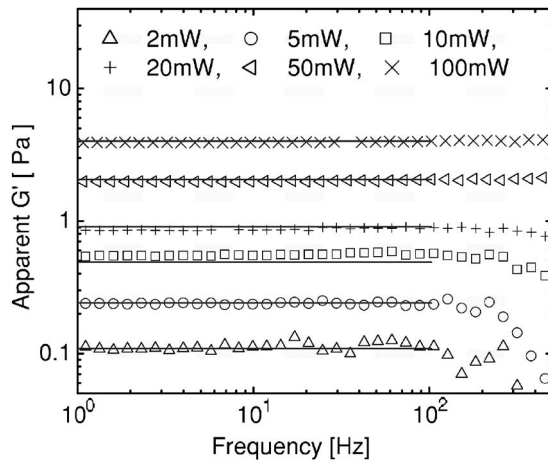
FIG. 5. *Apparent* storage moduli (caused by the trap) as a function of frequency, measured in water with 1PMR for different laser powers (measured before the objective, see text). The solid lines are the theoretical predictions based on the measured trap stiffnesses.

$f = \omega/2\pi$ for different laser powers. As the laser power is increased, the rms amplitude (area under the curve) of the position fluctuations becomes smaller, similar to the behavior observed for a particle in water. Due to the viscoelastic nature of the *fd* solution, the autocorrelation functions of one particle are not Lorentzian [20], but, as in water, the spectra $S^{(1)}$ for all the different laser powers coincide at frequencies larger than a characteristic frequency that is linearly dependent on the trap strength.

To highlight the systematic effect of the laser trap on the data, we calculated the storage modulus $G'(2\pi f)$ as measured by the 1PMR method without first removing the effect of the trap [Fig. 7(a) and 7(b)]. These data were obtained with the same particle size and laser power settings as the water data in Fig. 6. The trap stiffnesses were calculated from the fluctuations of trapped particle from the same batch at the same laser powers in buffer as mentioned above. The *uncorrected* G' increase proportionally to the laser intensity
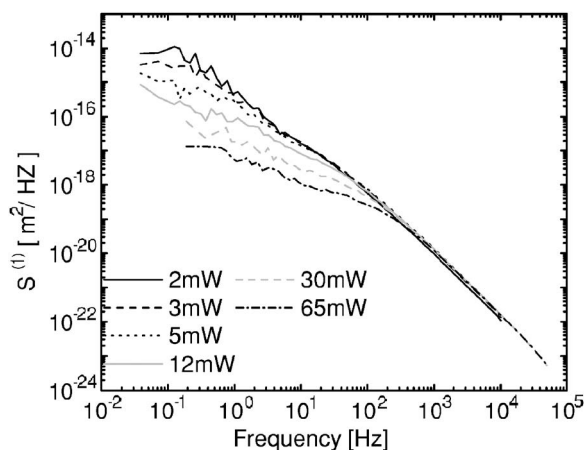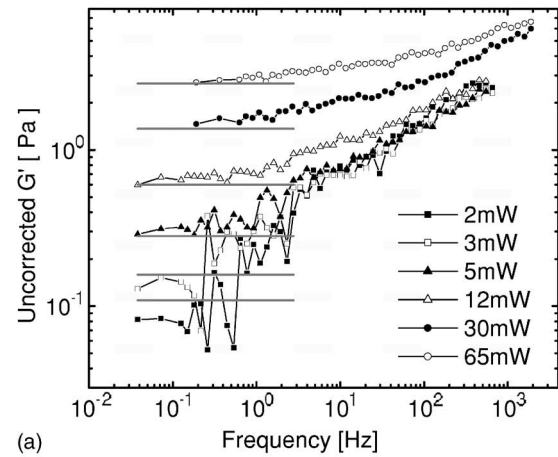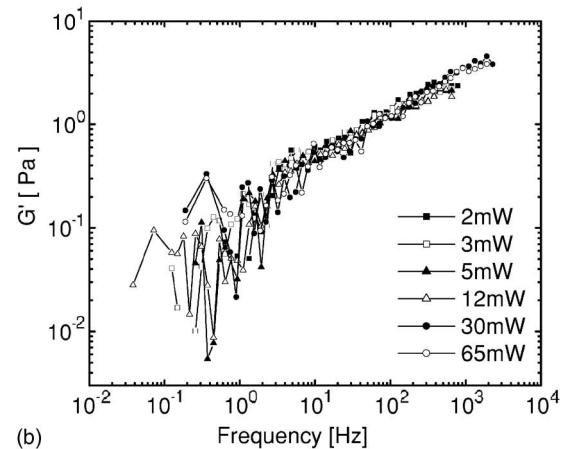

FIG. 6. Displacement autocorrelations as a function of frequency of a particle of radius $R = 0.58 \ \mu$m in a 10 mg/ml *fd* virus solution for different laser intensities (measured before the objective, see legend). The sampling rate was 100 kHz.

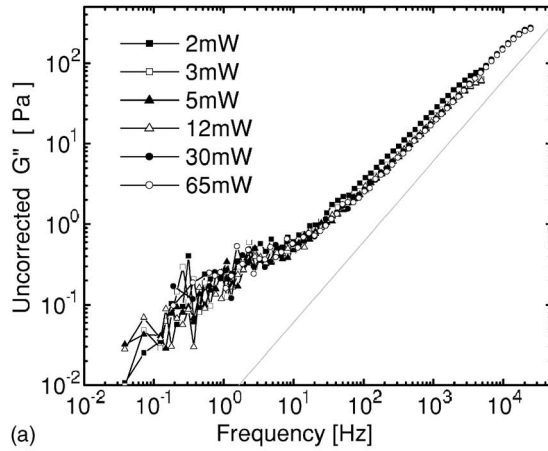FIG. 7. (a) *Uncorrected* storage moduli G' for a 10 mg/ml *fd* solution measured with 1PMR using different laser powers (measured before the objective, see legend). The gray lines are the expected moduli corresponding to the G' measured in water for the same power settings. (b) *Actual* storage moduli G' calculated using the response functions corrected for the traps using Eq. (7a). (Data are shown versus frequency, $f = \omega/2\pi$).
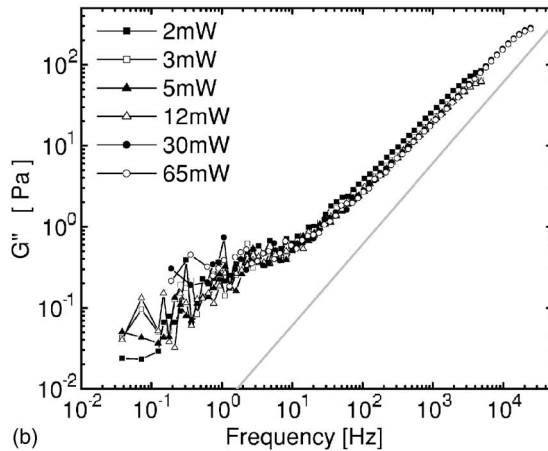
at low frequencies. The *uncorrected* moduli, determined using low power settings (3, 7, and 15 mW), converge at high frequencies to the *actual* storage modulus [Fig. 7(b)] of the medium. At larger laser powers (25, 70, and 150 mW), the *uncorrected* storage moduli are affected by the trap up to the largest probed frequency of 2 kHz. At low frequencies the trap dominates the moduli which can be seen from the comparison to grey lines in Fig. 7 reflecting the pure trap effect.

We used Eq. (7a) to correct the *measured* single-particle response functions $\chi^{(1)}$ for the trap effect, and obtain the single-particle response functions $\alpha^{(1)}$. We then applied Eq. (4) to calculate the complex shear moduli G. The results for the storage modulus G' are plotted in Fig. 7(b). As expected, the moduli G' fall onto one curve for all laser powers, which represents the storage modulus of the *fd* solution [20].

The *uncorrected* loss moduli G'' from 1PMR at various laser powers are plotted in Fig. 8(a). There is no significant effect from the trapping laser on the *uncorrected* G'', and all the measurements fall onto one curve even before correction, which does not change much with correction [Fig. 8(b)]

FIG. 8. (a) *Uncorrected* loss moduli G'' and (b) *actual* loss moduli G'' [obtained with Eq. (7a)], measured in x direction with 1PMR for a 10 mg/ml fd solution for different laser powers (measured before the objective, see legend). The gray line shows the loss modulus of the buffer. The trapping laser does not have a significant effect on G''.

(since G'' is negative, we report its absolute value in all figures).

We note that, in order to record the single- and interparticle response functions simultaneously, in all of these measurements two particles are trapped, so both $k^{(1)}$ and $k^{(2)}$ have nonzero values. In measurements with just one trapping laser ($k^{(1)} \neq 0$ and $k^{(2)} = 0$), Eq. (7a) simplifies to $1/\alpha^{(1)} = 1/\chi^{(1)} - k^{(1)}$.

We conclude that to correct for the trap effect in 1PMR and to get the *actual* storage modulus of a viscoelastic solution, it is sufficient to subtract a constant of $k/(6\pi R)$ from the *uncorrected* storage modulus.

B. Two-particle microrheology

To obtain the shear modulus of a medium from 2PMR we calculate the cross-correlation displacement of two hydrodynamically coupled particles trapped in two separate laser foci. In this case the correction for trap effects becomes slightly less straightforward.

Again, we first show data for particles trapped in water, as a purely viscous fluid. The Fourier transforms of the cross-
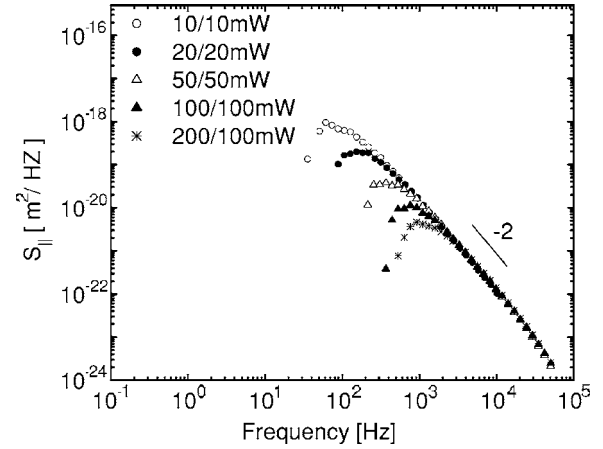

FIG. 9. Inter-particle displacement correlation functions as a function of frequency, $f = \omega/2\pi$ of a pair of particles (radius $R = 0.58$ μm) separated by a distance $r = 2.9$ μm, trapped with different laser powers in water. Laser intensities were varied in parallel in the two traps (measured before the objective, legend: 1064/830 nm powers). Low-frequency anticorrelations are not plotted in this ln-ln plot. At high frequencies, all curves superimpose onto one curve with slope −2.

correlation functions, $S_{\parallel,\perp}(2\pi f)$, of two thermally fluctuating particles in a viscous solution have a power-law slope of −2 at high frequencies just as was the case for single particles [21]. Figure 9 shows inter-particle correlation function ($S_{\parallel}$) obtained using Eq. (2) at different laser powers for both traps with the trap stiffness of both traps as shown in Fig. 2. At low frequencies, where the confinement by the traps is dominant, the motion of the particles becomes anticorrelated, i.e., $S_{\parallel}$ becomes negative (not visible in the ln-ln plot). At high frequencies, the viscous drag is dominant so that the $S_{\parallel}$ are independent of trap power and overlap with a (power law) slope of −2.

Figures 10(a) and 10(b) show linear-ln plots of the *measured* real and imaginary parts of the inter-particle response functions $\chi'_{\parallel}$ and $\chi''_{\parallel}$ for different powers. Using an approach similar to that of the previous section, we calculated $\chi_{\parallel}$ in water from Eq. (6c). The predictions from the measured trap stiffnesses (lines) are in good agreement with the measured $\chi'_{\parallel}$ and $\chi''_{\parallel}$. It is evident that the maxima in $\chi'_{\parallel}$ shift up in frequency and down in amplitude with increasing the laser power. This can be calculatedformally from Eq. (6c) with the Stokes assumption for the frequency of the maximum of $\chi'_{\parallel}$ which corresponds to the frequency of the zero crossing of the $\chi''_{\parallel}$: $f_{Max} = (\sqrt{k^{(1)}k^{(2)}[4 - 9(R/r)^2]})/24\pi^2 \eta R$ and for the amplitude of the maximum: $\chi^{(1)}_{Max} = 3k^{(2)}/[2Rk^{(1)}(k^{(1)} + k^{(2)})]$.

The apparent storage and loss moduli calculated from the response functions $\chi'_{\parallel}$ and $\chi''_{\parallel}$ at various trapping powers without correcting for the laser trapping potentials are plotted in Fig. 11(a) and 11(b). As expected, in water this results in a constant *apparent* G' which is entirely due to the laser traps [Fig. 11(a)]. Noise at low frequencies is due to laser beam pointing fluctuations and is particularly visible for the higher laser intensities because the particle fluctuations are smaller.

The (apparent) loss moduli G'' for different laser powers calculated from the uncorrected response functions are
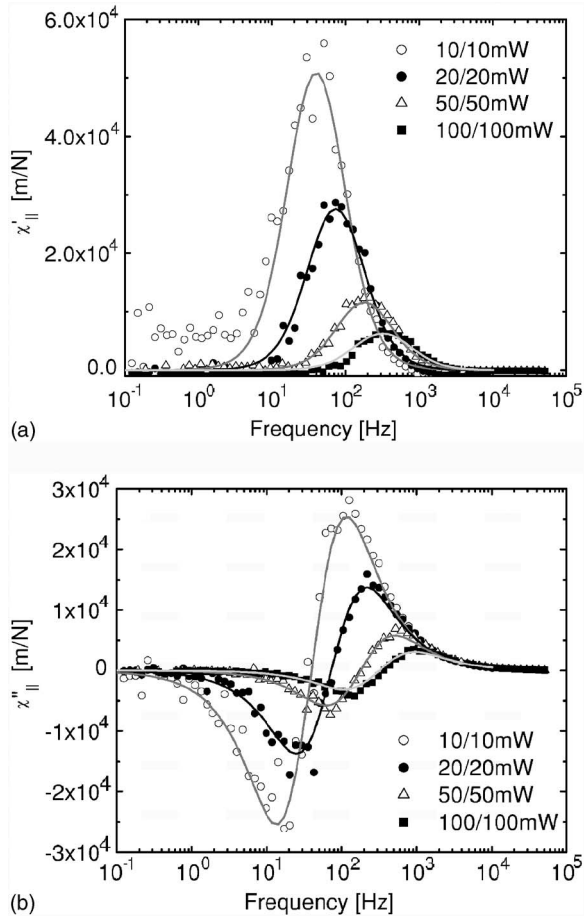
FIG. 10. (a) Real part and (b) imaginary part of the inter-particles response functions of two particles in water as a function of frequency, $f = \omega/2\pi$ in the parallel direction, trapped with different laser powers varied in parallel in the two traps (measured before the objective, legend: 1064/830 nm powers). The theoretical predictions of Eq. (6c), calculated with the trap stiffness determined from corner frequency are plotted for comparison (lines).
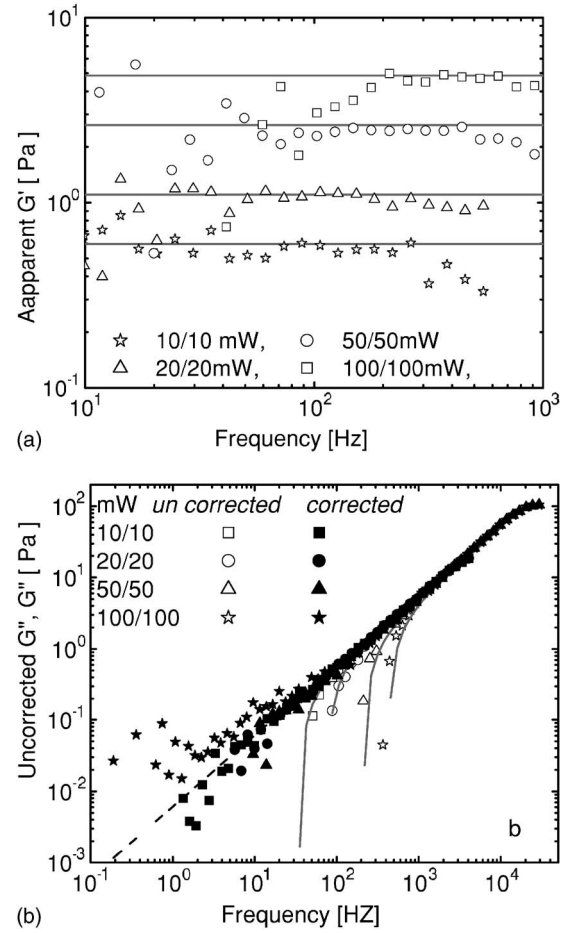

FIG. 11. (a) *Apparent* storage modulus G' and (b) *apparent* loss modulus G'' (empty symbols) measured in parallel direction with 2PMR in water as a function of frequency, $f = \omega/2\pi$ with different laser powers varied in parallel in the two traps (measured before the objective, legend: 1064/830 nm powers). The gray lines are the calculated *apparent* moduli G' and G'' from the predicted response $\chi_\parallel$ as in Eq. (6c). Filled symbols in (b) show the corrected loss modulus of water calculated using $\alpha_\parallel$ and the expected loss modulus for water, $G''(f) = -2\pi f \eta$ plotted as a broken line.

shown in Fig. 11(b). The frequency-dependent anticorrelation of $\chi_\parallel''$ caused by the trap (shown in Fig. 10) is observed here as missing data points at low frequencies in the ln-ln plot of G''. The solid gray lines in both figures show the theoretical predictions of the apparent moduli determined from the uncorrected response functions $\chi_\parallel''$ and $\chi_\parallel''$ using measured trap stiffnesses and Stokes assumptions in water.

In Figures 11(a) and 11(b), we obtain the *actual* moduli G' and G'' from $\alpha_\parallel'$ and $\alpha_\parallel''$, the corrected response functions according to Eq. (7c). The storage modulus G' is scattered around an average value of close to 0, as expected for water (data not shown); G'' now extends to lower frequencies. The data are consistent with the expected value of $G''(f) = -2\pi f \eta$ for water, plotted as a broken line.

Finally, we examined the effect of the traps on the inter-particle response functions in viscoelastic solutions of *fd* virus. Fig. 12 shows $S_\parallel$ for different laser powers. At high frequencies all curves fall on top of each other, as expected. At low frequencies anticorrelated motion is observed again [negative values of $S_\parallel$ not plotted], below a frequency that depends on the trap strength. The anticorrelation occurs at

frequencies that are about two decades smaller than for the same measurements in water due to the higher viscosity and elasticity of the *fd* solution.

Figures 13(a) and 13(b) compare the storage moduli of the *fd* solutions measured with 2PMR derived from uncorrected and from corrected response functions. Figure 13(a) shows the *uncorrected* results, while Fig. 13(b) shows the corrected or *actual* G'. The trap potentials make the *apparent* storage moduli G' approach a constant at low frequencies for high laser powers and change the slope of the curves at higher frequencies [Fig. 13(a)]. The curves for the corrected G' (corrected for both laser traps) collapse onto one curve for all laser powers [Fig. 13(b)], independent of trapping force.

Figures 14(a) and 14(b) demonstrate that the loss moduli of the *fd* solution measured with 2PMR are much less affected by the traps than the storage moduli. Figure 14(b) shows the *uncorrected* G'' derived from the uncorrected response functions, while Fig. 14(b) shows the *corrected* G''.
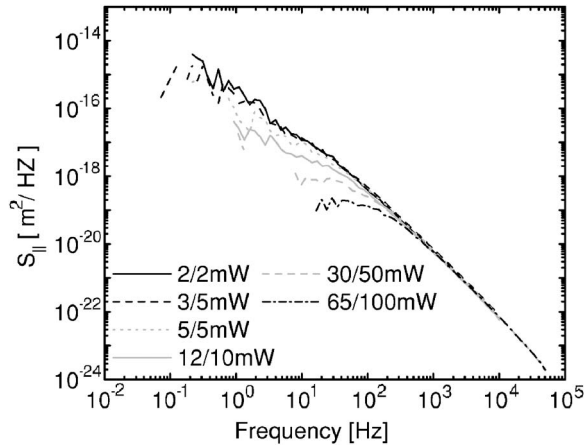
FIG. 12. Inter-particle correlation functions in the parallel direction of two particles separated by a distance $r = 2.9\ \mu$m in a 10 mg/ml *fd* solution, as a function of frequency. The trap powers were varied in parallel (measured before the objective, legend: 1064/830 nm powers). A power-dependent anticorrelation is observed at low frequencies.

The missing low-frequency range in the *uncorrected* case *of* G'' is due to the trap-induced anticorrelation, observed for a high power of 200 mW for $\lambda = 1064$ nm and 150 mW for $\lambda = 830$ nm. The trap correction to the response functions removes the anticorrelation effect and therefore extends the frequency range to lower frequencies [Fig. 14(b)].

As can be seen in Figures 7, 8, 13, and 14, noise in the results tends to become large below about 5 Hz. There is a multitude of reasons and possible cures for that, depending on the system studied and the method used. Averaging data decreases noise. Here we averaged 8 data sets taken over 80 s. A practical limit might be about 100 data sets. 2PMR results suffer from the $1/r$ decay of the signal and are therefore noisier than 1PMR results. Laser beam-pointing fluctuations tend to become relevant below a frequency that depends on the amplitude of the fluctuations of the probe particle which in turn depends on the viscoelastic modulus of the sample. Typically laser effects become noticeable below $\sim$1 Hz. Note furthermore that in all our figures we show the direct data, not smooth fits to the data. The latter is often done in the field, but it obscures the actual errors.

VI. DISCUSSION

Correlations in the motion of trapped particles in the time domain have been studied in purely viscous solutions before [30,31]. Hough and Ou-Yang [32] derived formally different but in essence equivalent results for the response functions.

Because we use correlated Brownian fluctuations in optical traps to measure viscoelastic properties of soft materials we need to correct for such additional correlations. We have here used our formal representation of single- and inter-particle response functions to develop a correction procedure for one and two particle microrheology. We have shown that it is straightforward to correct 1PMR results by subtracting a constant from $G'(\omega)$. If there is a second particle trapped in the vicinity, in principle, there will be an effect of both traps
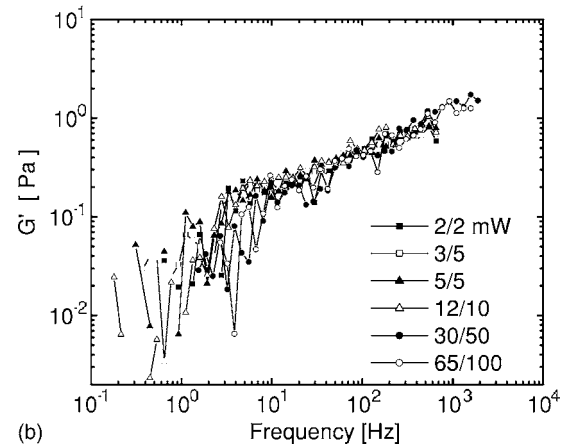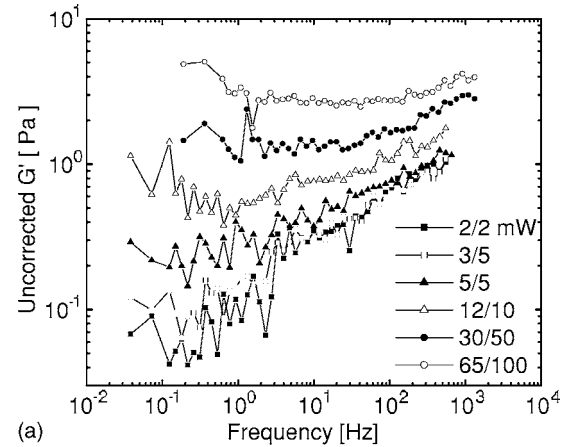

FIG. 13. Storage shear modulus of a 10 mg/ml *fd* solution as a function of frequency G', measured with 2PMR in parallel direction. The trap powers were varied in parallel (measured before the objective, legend: 1064/830 nm powers), with the (a) *uncorrected* modulus G' and (b) the *actual* modulus G' calculated using the corrected response functions in Eq. (7c).

on the observed particle. The effect of the second trap predicts an asymmetry in the measured response function, which was found to be negligible under the conditions $(R/r = 0.2)$ we used. In 2PMR, however, the effect of both traps on both particles has to be taken into account in a symmetric way. In 2PMR it is simpler to correct the particle response functions before calculating medium shear moduli. The correction is more involved, including higher order terms in the storage constants, even if linear elasticity is assumed. It is particularly notable and at first glance counter intuitive, that trapping two particles leads to anticorrelated fluctuations at low frequencies, an effect that is more pronounced in purely viscous media than in viscoelastic media. This is different from the anticorrelated fluctuations occurring at very high frequencies due to solvent inertia [33,34]. The Fourier transform of the cross-correlation function of particle displacement thus becomes negative at low frequencies (and cannot be ln-ln plotted as usual).

Intuitively, the anticorrelations seen at low frequency can be understood in the following way. For simple liquids, along any particular axis, the thermal position fluctuations of two particles (1 and 2) around the centers of their respective
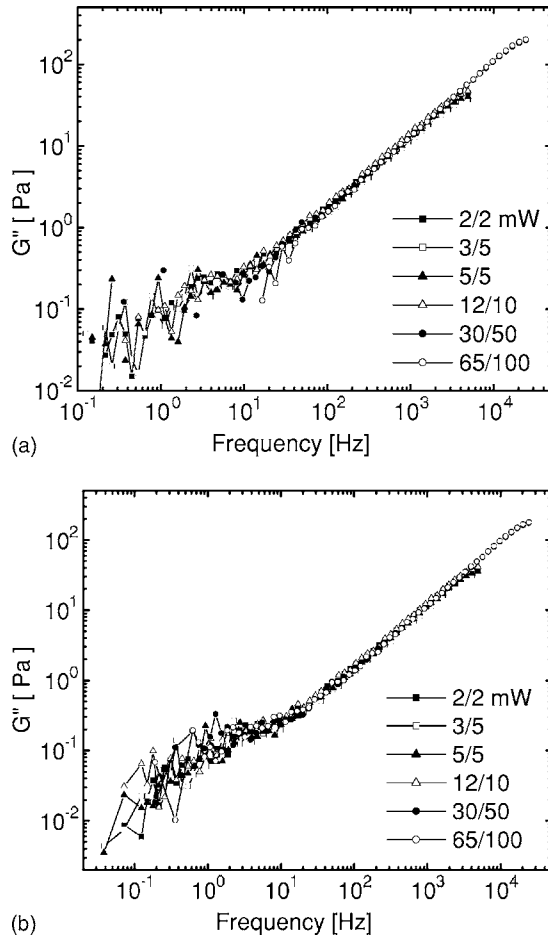
FIG. 14. Loss moduli of a 10 mg/ml fd solution as a function of frequency G'', measured with 2PMR in the parallel direction. The trap powers were varied in parallel (measured before the objective, legend: 1064/830 nm powers). The *uncorrected* G'' in (a) and *actual* modulus in (b) G' calculated using the corrected response functions [Eq. (7c)] do not show a significant difference for the lower powers. For higher laser powers 25/50, 70/70, and 200/150 mW correction eliminates the negative values at low frequencies [not plotted in (a)].

optical traps can be transformed into a relative coordinate system by $x_s = \frac{1}{2}(x_1 + x_2)$ and $x_a = \frac{1}{2}(x_1 - x_2)$, where x_s describes the in- phase and x_a the out of phase motion. Since the motion at the colloidal scale is strongly over damped, both amplitudes on average decay exponentially. Due to the hydrodynamic interactions between the two particles, the out of phase amplitude experiences a greater drag or dissipation and thus decays more slowly. Furthermore, as noted in Ref. [30], since the mean-square amplitudes of the two modes are equal, the correlation function $\langle x_1(t)x_2(0)\rangle$ is at all times dominated by the anticorrelated mode. More precisely

$$\langle x_1(t)x_2(0)\rangle \propto k_B T(e^{-t/\tau_s} - e^{-t/\tau_a}), \qquad (9)$$

is always negative, where $\tau_s < \tau_a$ are the decay rates of the two modes.

By contrast, when plotting correlation functions in the frequency domain, as we do in our experiments, the correlations are negative at low frequency and positive at high frequency. This is because the faster decaying symmetric mode has greater high-frequency content. More precisely, the Fourier-transformed correlation function

$$\int dt \langle x_1(t)x_2(0)\rangle e^{i\omega t} \propto k_B T\left(\frac{\tau_s}{1 + (\omega\tau_s)^2} - \frac{\tau_a}{1 + (\omega\tau_a)^2}\right),$$
$$(10)$$

is positive for large ω and negative for small ω.

Equivalently, this can be seen from a simple force-balance argument. At high frequencies, the forces due to the viscoelastic medium dominate the trapping forces, and the instantaneous propagation of stress means that one particle tends to move with the other. At frequencies below the characteristic relaxation time of a single trapped particle, however, the trapping forces tend to dominate. This means that when one particle is displaced to one side of its trap, the restoring force from the trap, which is directed in the direction opposite to the displacement, is transmitted by the medium to the second particle. The second particle in turn is at this frequency effectively undamped in its motion in response to the first particle, i.e., it has time to relax in its own trap to equilibrium. This means that it will be displaced to the opposite side of its trap. The frequency scale for the crossover from anticorrelated to (positively) correlated motion and/or fluctuations is determined by the relaxation frequency of a single particle in its trap. This frequency will increase with increasing laser power (observed above), and is also expected to decrease for more viscoelastic media (also observed above). Furthermore, since the anticorrelations are the direct result of the traps, they also tend to disappear (or shift to lower frequencies) with increasing storage modulus of the medium.

With the rigorous and complete correction procedure we have developed here it is simple to extract the true medium response parameters from either particle fluctuation recordings or responses to actively driven particles when optical trapping is used. We have applied these methods in microrheology experiments presented in references [20,15,35,36]. In these experiments the laser powers were high enough to hold particles far from surfaces as well as preventing the diffusion of particles from the trap. In our experiment with actin [5], the laser power was low and the moduli were so high that a correction was not necessary.

We expect the method we have developed in this paper to be useful in applications of laser-interferometry based active and passive microrheology in many different soft media.

[1] R. G. Larson, *The Structure and Rheology of Complex Fluids* (Oxford University Press, Oxford, 1998).

[2] T. G. Mason and D. A. Weitz, Phys. Rev. Lett. **75**, 2770 (1995).

[3] T. G. Mason, K. Ganesan, J. H. Van Zanten, D. Wirtz, and S. C. Kuo, Phys. Rev. Lett. **79**, 3282 (1997).

[4] F. Gittes, B. Schnurr, P. D. Olmsted *et al.*, Phys. Rev. Lett. **79**, 3286 (1997).

[5] B. Schnurr, F. Gittes, F. C. MacKintosh *et al.*, Macromolecules **30**, 7781 (1997).

[6] A. J. Levine and T. C. Lubensky, Phys. Rev. Lett. **85**, 1774 (2000).

[7] F. C. MacKintosh and C. F. Schmidt, Curr. Opin. Colloid Interface Sci. **4**, 300 (1999).

[8] A. W. C. Lau, B. D. Hoffman, A. Davies, J. C. Crocker, and T. C. Lubensky, Phys. Rev. Lett. **91**, 198101 (2003).

[9] F. G. Schmidt, B. Hinner, E. Sackmann *et al.*, Phys. Rev. E **62**, 5509 (2000).

[10] L. Starrs and P. Bartlett, Faraday Discuss. **123**, 323 (2003).

[11] J. C. Crocker, M. T. Valentine, E. R. Weeks *et al.*, Phys. Rev. Lett. **85**, 888 (2000).

[12] A. J. Levine and T. C. Lubensky, Phys. Rev. E **63**, 041510 (2001).

[13] D. T. Chen, E. R. Weeks, J. C. Crocker *et al.*, Phys. Rev. Lett. **90**, 108301 (2003).

[14] M. W. Allersma, F. Gittes, M. J. deCastro *et al.*, Biophys. J. **74**, 1074 (1998).

[15] M. Buchanan, M. Atakhorrami, J. F. Palierne *et al.*, Phys. Rev. E **72**, 011504 (2005).

[16] J. C. Crocker and D. G. Grier, J. Colloid Interface Sci. **179**, 298 (1996).

[17] F. Gittes and C. F. Schmidt, Biophys. J. **74**, A183 (1998).

[18] E. J. G. Peterman, M. A. van Dijk, L. C. Kapitein *et al.*, Rev. Sci. Instrum. **74**, 3246 (2003).

[19] J. Sambrook, E. F. Fritsch, and T. Maniatis, *Molecular Cloning: A Laboratory Manual* (Cold Spring Harbor Laboratory Press, Cold Spring Harbor, 1989).

[20] K. M. Addas, C. F. Schmidt, and J. X. Tang, Phys. Rev. E **70**, 021503 (2004).

[21] M. Atakhorrami *et al.* (unpublished).

[22] F. Gittes and C. F. Schmidt, Opt. Lett. **23**, 7 (1998).

[23] F. Gittes and C. F. Schmidt, in *Methods in Cell Biology* (Academic Press, 1998), Vol. 55, p. 129.

[24] L. D. Landau and E. M. Lifshitz (1980).

[25] T. G. Mason and D. A. Weitz, Phys. Rev. Lett. **74**, 1250 (1995).

[26] K. Berg-Sørensen and H. Flyvbjerg, Rev. Sci. Instrum. **75**, 594 (2004).

[27] Keir C. Neuman and S. M. Block, Rev. Sci. Instrum. **75**, 2787 (2004).

[28] L. D. Landau and E. M. Lifshitz, *Fluid Mechanics* (Butterworth-Heinemann, Oxford, 2000).

[29] C. W. Oseen, *Neuere Methoden und Ergebnisse in Der Hydrodynamik* (Leipzig Akademische Verlagsgesellschaft, Leipzig, 1927).

[30] J. C. Meiners and S. R. Quake, Phys. Rev. Lett. **82**, 2211 (1999).

[31] S. Henderson, S. Mitchell, and P. Bartlett, Phys. Rev. E **64**, 061403 (2001).

[32] L. A. Hough and H. D. Ou-Yang, Phys. Rev. E **65**, 021906 (2002).

[33] M. Atakhorrami, G. H. Koenderink, C. F. Schmidt *et al.*, Phys. Rev. Lett. **95**, 208302 (2005).

[34] T. B. Liverpool and F. C. MacKintosh, Phys. Rev. Lett. **95**, 208303 (2005).

[35] M. Buchanan, M. Atakhorrami *et al.*, Macromolecules **38**(21), 8840 (2005).

[36] M. Atakhorrami and C. F. Schmidt, Rheologica Acta (to be published).

[37] G. H. Koenderink *et al.*, Phys. Rev. Lett. **96**, 138307 (2006).